AGU PUBLICATIONS

Paleoceanography

RESEARCH ARTICLE
10.1002/2013PA002506

Key Points:
- EEP thermocline deep during the late Miocene small Dictyococcites acme
- Low eccentricity favorable for the small *Dictyococcites* spp. growth

Correspondence to:
C. Beltran,
catherine.beltran@upmc.fr

Citation:
Beltran, C., G. Rousselle, J. Backman, B. S. Wade, and M. A. Sicre (2014), Paleoenvironmental conditions for the development of calcareous nannofossil acme during the late Miocene in the eastern equatorial Pacific, *Paleoceanography*, *29*, doi:10.1002/2013PA002506.

Received 14 MAY 2013
Accepted 16 JAN 2014
Accepted article online 21 JAN 2014

Paleoenvironmental conditions for the development of calcareous nannofossil acme during the late Miocene in the eastern equatorial Pacific

Catherine Beltran[1,2], Gabrielle Rousselle[1,2], Jan Backman[3], Bridget S. Wade[4], and Marie Alexandrine Sicre[5,6]

[1]UPMC Université Paris 06, UMR CNRS 7193 ISTeP, 4 Place Jussieu, 75005, Paris, France, [2]CNRS, UMR CNRS 7193 ISTeP, 4 Place Jussieu, 75005, Paris, France, [3]Department of Geology and Geochemistry, Stockholm, Sweden, [4]Department of Earth Sciences, University College London, London, UK, [5]Laboratoire des Sciences du Climat et de l'Environnement, IPSL, CNRS/CEA/UVSQ, Gif-sur-Yvette, France, [6]Sorbonne Universités (UPMC, Univ Paris 06)-CNRS-IRD-MNHN, LOCEAN Laboratory, 4 place Jussieu, F-75005, Paris, France

Abstract Repeated monospecific coccolithophore dominance intervals (acmes) of specimens belonging to the *Noelaerhabdaceae* family—including the genus *Reticulofenestra* and modern descendants *Emiliania* and *Gephyrocapsa*—occurred during the Neogene. Such acme was recognized during the late Miocene (~ 8.6 Ma), at a time of a major reorganization of nannofossil assemblages resulting in a worldwide temporary disappearance of larger forms of the genus *Reticulofenestra* (*R. pseudoumbilicus*) and the gradual recovery and dominance of its smaller forms (< 5 μm). In this study we present a multiproxy investigation of late Miocene sediments from the east equatorial Pacific Integrated Ocean Drilling Program Site U1338 where small reticulofenestrid-type placoliths with a closed central area—known as small *Dictyococcites* spp. (< 3 μm)—formed an acme. We report on oxygen and carbon stable isotope records of multispecies planktic calcite and alkenone-derived sea surface temperature. Our data indicate that, during this 100 kyr long acme, the east equatorial Pacific thermocline remained deep and stable. Local surface stratification state fails to explain this acme and thus contradicts the model-based hypothesis of a Southern Ocean high-latitude nutrient control of the surface waters in the east equatorial Pacific. Instead, our findings suggest that external forcing such as an extended period of low eccentricity may have created favorable conditions for the small *Dictyococcites* spp. growth.

1. Introduction

The late Miocene (11.6–5.3 Ma) is an apparently cryptic climatic warm interval characterized by weak meridional temperature gradients [*Flower and Kennett*, 1994; *La Riviere et al*., 2012] with small and dynamical ice sheets [*McKay et al*., 2009] under presumably low atmospheric CO_2 conditions [*Pearson and Palmer*, 2000; *Pagani et al*., 2005; *Foster et al*., 2012]. *La Riviere et al*. [2012] proposed that the combination of a globally deep thermocline and reduced low-latitude sea surface temperature gradients could partially explain the late Miocene warmth. The underlying causes for this oceanic configuration and globally elevated temperatures remain unidentified.

In this complex paleoclimatic context, between 9.1 Ma and 7.1 Ma, the calcareous nannofossil genus *Reticulofenestra*, major carbonate producer in the oceanic habitat [*Marlowe et al*., 1990; *Henderiks and Pagani*, 2007; *Plancq et al*., 2012], shows an abrupt decrease in their size known as the paracme of *Reticulofenestra pseudoumbilicus* [*Rio et al*., 1990]. This paracme interval was first reported in the Indian Ocean and subsequently recognized in the Atlantic and Pacific Oceans [*Takayama*, 1993; *Kameo and Bralower*, 2000]. At low latitudes, this event is identified by the temporary disappearance of the large *R. pseudoumbilicus* followed by the emergence and dominance of small (<5 μm) monospecific specimens (acme), while at higher latitudes, medium-sized populations persisted.

Successions of similar acmes of species belonging to the *Noelaerhabdaceae* family—including the genus *Reticulofenestra* and modern descendants *Emiliania* and *Gephyrocapsa*—have been reported to last for several tens of thousands of years during the past 10 Ma [*Marlowe et al*., 1990; *Young et al*., 1992; *Bollmann et al*., 1998]. The mechanism for these acmes remains poorly understood.

The modern ocean distribution of coccolithophores is controlled by several factors, e.g., light, temperature, nutrients, and water stratification [*Winter and Siesser*, 1994]. Changes in the ocean circulation or climate conditions

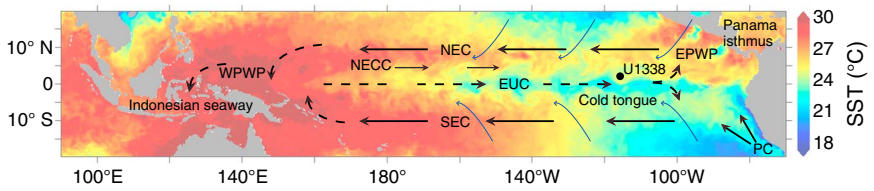

Figure 1. Equatorial Pacific map showing the position of IODP 321 Site 1338, the general modern surface and subsurface currents and the mean annual sea surface temperatures across the equator [*Levitus and Boyer*, 1994]. PC: Peru current, NEC: north equatorial current, SEC: south equatorial current, EUC: equatorial under current, NECC: north equatorial counter current, WPWP: west Pacific warm pool, EPWP: east Pacific warm pool.

thus influence coccolithophore growth. Parameters such as (1) nitrate and phosphate concentrations, (2) variations in carbon or calcium budget with residence times of 100 kyr and 1 Myr, respectively, and (3) the ocean silica budget (controlled by continental input and/or by the silica leakage mechanism) [e.g., *Matsumoto et al*., 2002] control the relative success of coccolithophores versus diatoms and provide possible optimal environmental conditions for rapid coccolithophore development. Environmental conditions have been proposed to explain the small *Gephyropcapsa* acme zone reported by *Gartner* [1988] from 0.93 to 1.25 Ma. *Rickaby et al*. [2007] attributed the Pleistocene *Gephyrocapsa caribbeanica* and *Emiliania huxleyi* acmes to the orbital control (eccentricity) on the silica leakage and the phytoplankton growing season length as well as the nutrient supply from continental weathering. Alternatively, *Bollmann et al*. [1998] considered that the main cause for the dominance of *Gephyrocapsa* during the middle Pleistocene and the *E. huxleyi* acme in the modern ocean depicts an evolutionary adaptation to environmental stress.

Here our main objective was to identify the environmental drivers of coccolithophore distributions, including acme intervals of small reticulofenetrids during the late Miocene [*Backman*, 1980; *Marlowe et al*., 1990; *Young*, 1990; *Aubry*, 1992; *Beaufort*, 1992; *Henderiks*, 2008; *Pälike et al*., 2010]. Our study focuses on the eastern equatorial Pacific Integrated Ocean Drilling Program (IODP) Site U1338, where small reticulofenestrid-type placoliths with a closed central area represent >80% of the total calcareous nannofossil assemblage, around 8.6 Ma. These morphotypes are often referred to small *Dictyococcites* spp. (<3 μm).

Although coccolithophores are major carbonate producers, their use as seawater chemistry recorder has been limited mostly because their separation from the bulk carbonate is time-consuming task due to their small size. In this study, we use the *Minoletti et al*. [2009] separation technique designed for concentrating calcareous nannofossils to perform oxygen and carbon isotopic (δ^{18}O, δ^{13}C) measurements. We combined the alkenone-derived sea surface temperatures (SSTs), δ^{18}O, and δ^{13}C of calcareous nannofossils and planktic foraminifera species with distinct depth habitats (mixed layer and upper thermocline dweller) to develop the first holistic understanding of the surface to thermocline and nutricline structure of the late Miocene equatorial Pacific Ocean during the small *Dictyococcites* spp. acme period.

2. Oceanographic Setting

Today, the equatorial Pacific is characterized by strong east-west sea surface temperature and productivity gradients (the warmer waters being found in the western equatorial Pacific warm pool (WPWP)) and an asymmetry of the thermocline depth (~ 50 m in the east and ~150 m in the west). The oceanic circulation in the eastern Pacific is mainly controlled by the Walker cell circulation and the NE trade winds [*Cannariato and Ravelo*, 1997; *Kamikuri et al*., 2009]. The resulting westward flowing south and north equatorial currents (SEC and NEC, respectively) (Figure 1) cause surface waters to pile up in the west Pacific warm pool (WPWP). The consequent eastward pressure force [*Philander*, 1980; *Stewart*, 2005] leads to the equatorial under current (EUC) flowing 50 to 250 m below the surface that shoals eastward in the eastern equatorial cold tongue.

The nitrate, iron, and silicate contents of the equatorial undercurrent (EUC) that originate in part from the sub-Antarctic mode waters (SAMW) [*Toggweiler et al*., 1991] are considered as the dominant control on the east equatorial sea surface water productivity [*Loubere*, 2000].

The eastern equatorial Pacific (EEP) surface productivity is characterized by the alternation of silica rich versus carbonate-rich sedimentation resulting from the alternate accumulation of diatoms (glacial) and coccolithophore (interglacial). These shifts in phytoplankton community at low latitudes have been attributed

to the "Silica Leakage Hypothesis" [*Matsumoto et al*., 2002]. During interglacial times, the phytoplankton species change from diatoms to coccolithophores as a result of a low $Si(OH)_4$ supply from the high latitudes where, under present Fe-limited conditions, diatoms silicify heavily [*Franck et al*., 2000] and use up most of the Si upwelled around Antarctica. During glacial, when Fe is not limited, $Si(OH)_4$ that is not consumed can be transported in the SAMW and feed the EEP thus favoring the diatom production over coccolithophores [*Brown and Yoder*, 1994; *Egge and Aksnes*, 1992].

Sediments at the IODP Site U1338 were deposited above the calcite compensation depth on an 18 Ma old crust and remained in the equatorial zone (± 2° of the equator) during the Miocene and Pliocene (18 to 3 Ma) [*Pälike et al*., 2010]. Today, the core is located between the warm waters of the East Equatorial Warm Pool (EEWP) to the North, and the Cold Tongue around 1°S [*Deser and Wallace*, 1990] (Figure 1).

We aim to reconstruct paleoceanographic change during the small *Dictyococcites* spp. acme through an integrated geochemical study using multiple species of planktic foraminifera coupled with nannofossil size segregated oxygen and carbon isotopes and alkenone-derived sea surface temperature.

3. Material and Methods

3.1. Sample Location and Collection

The 415 m thick sediment sequence at Site U1338 (2°30.469'N, 117°58.178'W—4200 m water depth) consists of well-preserved biogenic oozes [*Fox and Wade*, 2013] dominated by calcareous nannofossils with variable contributions of foraminifera, diatoms, and radiolaria. In the late Miocene to early Pliocene, several intervals show dominance of *Dictyococcites* <3 μm or small *Sphenolithus* spp. We analyzed 50 samples from core U1338C-20H, corresponding to the acme of small *Dictyococcites* spp. (<3 μm) above the base of the *R. pseudoumbilicus* paracme, which was identified between samples U1338C-20H-6-110 cm and U1338C-20H-CC within Zone NN10 [*Pälike et al*., 2010]. A ~10 kyr temporal resolution was used in the interval from 8.81 Ma to 8.38 Ma.

3.2. Methods

Calcareous nannofossil assemblage counts were conducted following methods described by *Backman and Shackleton* [1983] and *Flores et al*. [1995]. All counts were performed using a Zeiss Axioscope cross-polarizing microscope at 1600X magnification. On average, 580 nannofossils were counted for each smear slide. In order to capture the full variability of the upper water column, stable isotope measurements were conducted on two planktic foraminifera species *Globorotalia menardii* and *Dentoglobigerina venezuelana*. *D. venezuelana* isotopic measurements were restricted to the 300–355 μm size fraction (as in *Wade et al*. [2007]). These species were present throughout the study interval, though *G. menardii* was too rare in some horizons to perform reliable isotope measurements.

Mixed calcareous nannofossil fine fraction (NF) dominated by *Coccolithus pelagicus* and *Calcidiscus leptoporus* was isolated using the *Minoletti et al*. [2009] separation technique. Additional smear slides of the NF fractions were prepared and about 200 liths were counted and measured in light microscopy using a cross-grid graticule to quantify the taxonomic compositions. Counts and size measurements were converted into volume contribution of each species following the approach of *Young and Ziveri* [2000] using given shape factors and average length for each nannofossil species. Because the separation technique is time consuming, $\delta^{18}O$ and $\delta^{13}C$ measurements on the NF fractions were carried out only on 16 samples (Table 2) to assess the evolutionary trends of the environmental conditions in the photic zone.

Oxygen and carbon stable isotope measurements were performed on a Finnigan Delta E mass spectrometer. CO_2 was extracted with anhydrous orthophosphoric acid at 50°C. The $\delta^{18}O$ and $\delta^{13}C$ values are expressed in per mil relative to the V-PDB standard reference (Vienna PeeDee Belemnite). The analytical precision is estimated to be ±0.1‰ for $\delta^{18}O$ and ±0.05‰ for $\delta^{13}C$.

The C_{37} alkenone concentrations were determined on the entire sample set (50 samples). About 6 g of sediment was freeze dried, extracted with organic solvents, and partitioned into compound classes by silica gel chromatography following the procedure of *Sicre et al*. [2001]. Gas chromatographic analyses were performed using a Varian 3400CX series equipped with a Septum Programmable Injector and a flame ionization detector

Table 1. Age and Depth of Datum From Site U1338 Used for the Age Model in This Study[a]

	Datum	Age (Ma)	Depth (CCCSF-A)	Depth Error
D	T *Thalassiosira burckliana*	7.84	161.17 m	0.97 m
N	B *Discoaster berggrenii*	8.29	164.25 m	0.625 m
D	T *Thalassiosira yabei*	8.44	173.3 m	0.75 m
R	T *Botryostrobus miralestensis*	8.59	179.9 m	1.48 m
R	B *Didymocyrtis penultima*	8.51	179.9 m	1.48 m
R	B *Spongaster bermingahami*	8.76	183.0 m	1.94 m
M	C4An/C4Ar.1r	9.098	189.39 m	

[a]Ages for polarity chrons (M) and for base (B) and top (T) occurrences of calcareous nannofossils (N), diatoms (D), and radiolarians (R) and their depths are from *Pälike et al.* [2010]. No planktic foraminiferal bioevents were useful in the studied interval because many marker taxa had rare or sporadic occurrences [*Hayashi et al.*, 2013]. All depths refer to the CCCSF-A (m) scale (meters compressed composite depth), corresponding to the corrected depth scale (CCSF-A) based on the splice by *Wilkens et al.* [2013], divided by a factor of 1.107 for conversion to CCCSF-A depths (refer to *Pälike et al.* [2010]).

using a fused silica capillary column (Chrompack CP Sil8, 50 m long, 0.32 mm internal diameter, 0.25 μm film thickness). Helium was used as a carrier gas. Alkenone concentrations were calculated using 5α-cholestane as an external standard added to the alkenone fraction prior injection. The $U^{k'}_{37}$ index ($U^{k'}_{37} = C_{37:2}/(C_{37:2} + C_{37:3})$ was calculated from the C_{37} alkenones to derive SSTs using the global calibration of *Conte et al.* [2006] $T = -0.957 + 54.293\ U^{k'}_{37} - 52.894\ (U^{k'}_{37})^2 + 28.321\ (U^{k'}_{37})^3$, providing better adjustment for warmer sea surface temperatures than the linear fit of *Prahl et al.* [1988]. The mean standard error of the estimated temperature is ±1.2°C [*Conte et al.*, 2006].

3.3. Age Model

The late Miocene average linear sedimentation rate at Site U1338 has been estimated from biomagnetostratigraphic at 2.2 cm/kyr [*Pälike et al.*, 2010]. Here we focus on the 171.92–180.82 m interval (Core 1338C-20H), falling between the top of *Thalssiosira burckliana* (161.17 m; 7.84 Ma) [*Backman et al.*, 2013] and the Chron C4An/C4Ar.1r boundary (189.39 m; 9.098 Ma) [*Pälike et al.*, 2010]. During this interval, the available age diagnostic data (calcareous nannofossil, diatom, radiolaria, and magnetostratigraphic) [*Pälike et al.*, 2010] do not perfectly fit the long-term age model. Therefore, an alternative biomagnetostratigraphic-based age model is presented (Table 1). Because of this discrepancy, we choose to present our data set versus depths. All depths refer to the CCCSF-A (m) scale (meters compressed composite depth) using the splice by *Wilkens et al.* [2013].

4. Results

4.1. Calcareous Nannofossil Assemblage Compositions

The calcareous nannofossil diversity along the studied interval is relatively low with a generally good to moderate preservation. However, three intervals show evidence of strong dissolution (179.64, 179.82, and 180.00 m). The assemblage composition is dominated by small *Dictyoccocites* spp. accounting on average for 66%. The second most abundant taxa, *Sphenolithus abies*, accounts for ~20% of the total assemblage. The other species that were identified in this interval (*Reticulofenestra haqii*, *Minylitha convallis*, *Calcidiscus leptoporus*, *Coccolithus pelagicus*, and *Discoaster* spp.) are minor (< 5% of the total assemblage).

Dominance of small *Dictyococcites* spp. is particularly pronounced between 177.46 and 175.94 m, whereas minor taxa (Figures 2a and 2b) remain low and show little variability.

Based on the $CaCO_3$ content at Site U1338 [*Lyle and Backman*, 2013], total calcareous nannofossil abundance, and the relative abundance of small *Dictyococcites* spp., five stratigraphic units (A–E) have been defined (Figure 2)

1. Unit A (180.82–178.81 m) is characterized by high $CaCO_3$ content varying between 60 and 75% and low calcareous nannofossil abundances. Small *Dictyoccocites* spp. dominate, accounting for 40 to 75% of the total assemblage.
2. Unit B (178.81–177.46 m) is defined by a concomitant increase of carbonate content and the number of calcareous nannofossils. Small *Dictyoccocites* spp. show a significant increase, up to 80% of the total assemblage by the end of the Unit B.

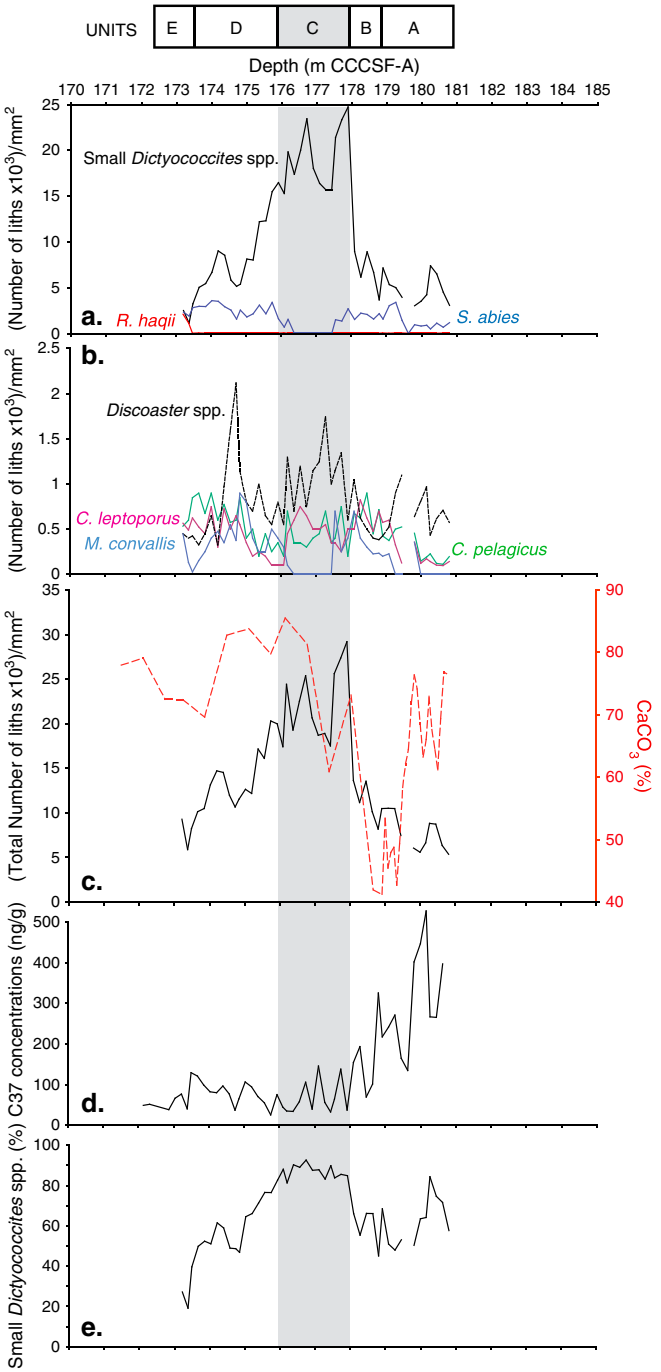

Figure 2. (a and b) Selected calcareous nannofossil absolute abundance record from Site U1338 given per mm^2. (c) Also reported the $CaCO_3$ content [*Lyle and Backman*, 2013] and the absolute total number of nannofossils. (d) The evolution of the C_{37} alkenone concentrations in the studied interval. (e) The grey-shaded unit C (see text for explanations) corresponds to the interval of maximum relative abundance of small *Dictyococcites* spp. in the calcareous nannofossil assemblage.

3. Unit C (177.46–175.94 m) corresponds to the maximum dominance of small *Dictyococcites* spp., representing on average 90% of the total assemblage. The total number of calcareous nannofossils and $CaCO_3$ contents (between 60 and 82%) are the highest.
4. Unit D (175.94–173.39 m) corresponds to the onset of the decrease of small *Dictyococcites* spp. relative abundances and of the number of calcareous nannofossils, while the carbonate content remains high (~ 75%).

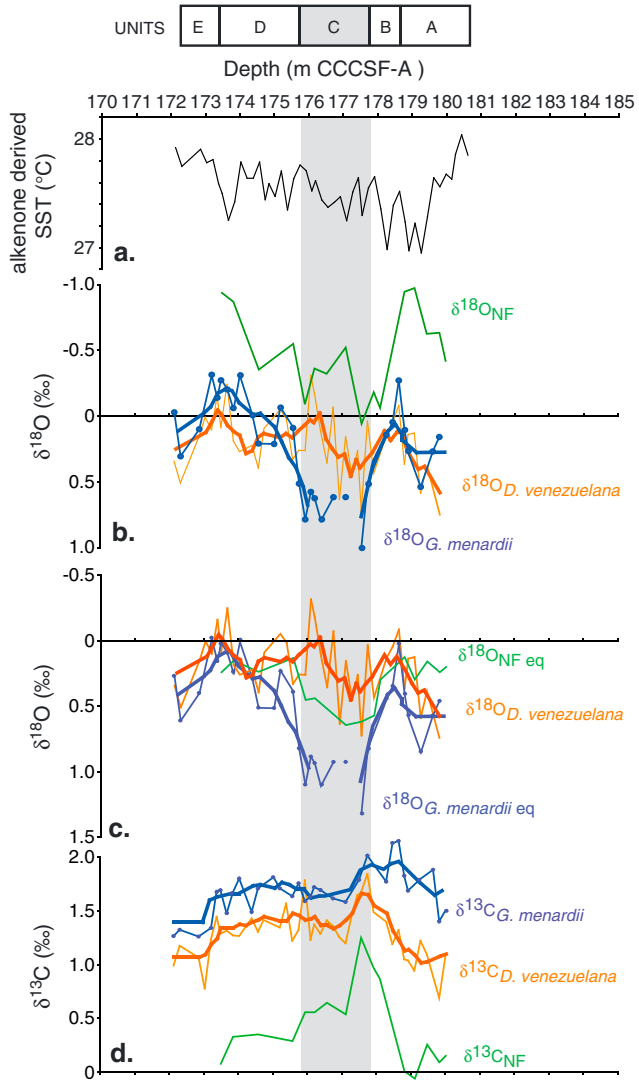

Figure 3. Alkenone-derived calculated (a) SSTs and (b) δ^{18}O, and (d) δ^{13}C signatures of the planktic foraminifera species *G. menardii* and *D. venezuelana* and the calcareous nannofossil separated fraction (NF), respectively, in blue, orange, and green. (c) Vital effect corrected δ^{18}O of calcareous nannofossil separated fraction NF (as discussed in the text and Table 2). The vital effect correction of +0.3‰ has been applied to the δ^{18}O values of *G. menardii*, [*Bouvier-Soumagnac and Duplessy*, 1985] (*D. venezuelana* has not been corrected). The thick blue and orange lines correspond respectively to the smoothed curves (5 points) for *G. menardii* and *D. venezuelana* obtained using Analyseries 2.0 [*Paillard et al.*, 1996]. The grey-shaded unit C corresponds to the maximum abundance interval of small *Dictyococcites* spp.

5. Unit E (from 173.39 m) is characterized by a significant contribution of *R. haqii* (20%), while small *Dictyococcites* spp. account for 20% and *S. abies* for 30% of the nannofossil assemblage. Similar to unit D, total calcareous nannofossils are low and carbonate content average 70%.

4.2. Alkenone Concentrations and SSTs

C_{37} alkenone concentrations (Figure 2d) vary between 24 and 526 ng/g of dry-weight sediment with a gradual decrease during units A and B. During intervals C to E, values remain stable and low ~ 70 ng/g. The $U^{k'}_{37}$ values range from 0.94 to 0.98, translating into SSTs varying between 27°C and 28°C (Figure 3a) which fall within the SST uncertainties. Accordingly, we consider that the SSTs remain stable, and high at 27–28°C, over the studied interval.

Table 2. Isotopic Signature of the NF Fraction ($\delta^{18}O_{NF}$) and Vital Effect Correction ($\delta^{18}O_{NF\ eq}$)[a]

Sample	Depth (m)	$\delta^{18}O_{NF}$ (Per Mil)	NF Fraction Composition (Volumic Percentage)			$\delta^{18}O_{NF\ eq}$ (Per Mil)
			C. leptoporus $l = 6\ \mu m$	*C. pelagicus* $l = 6\ \mu m$	Other[b]	
20H-2, 8	173.5	−0.94	24	65	11	0.25
20H-2, 48	173.86	−0.87	20	71	9	0.16
20H-2, 128	174.58	−0.35	24	66	10	0.25
20H-3, 88	175.58	−0.55	19	74	7	0.14
20H-3, 128	175.94	−0.09	35	55	10	0.46
20H-4, 8	176.21	−0.36	33	53	15	0.45
20H-4, 48	176.57	−0.32	38	50	12	0.53
20H-4, 108	177.11	−0.52	45	45	10	0.65
20H-5, 8	177.57	0.06	44	47	9	0.62
20H-5, 48	177.93	−0.18	39	46	15	0.58
20H-5, 68	178.11	−0.06	26	61	13	0.31
20H-5, 146	178.81	−0.94	17	67	16	0.13
20H-6, 28	179.1	−0.97	25	58	17	0.31
20H-6, 68	179.46	−0.62	20	71	9	0.17
20H-6, 108	179.82	−0.63	24	65	11	0.25
20H-6, 128	180	−0.41	22	68	10	0.21

[a]Relative volumic calcite contribution of the main coccolith species is reported. The mean length for *C. pelagicus* and *C. leptoporus* used for their volume calculations is *l* based on *Young and Ziveri* [2000] approach. The photic zone equilibrium isotopic signature estimation is $\delta^{18}O_{NF\ eq}$ using vital effect corrections of −1.1‰ for *C. leptoporus* [*Candelier et al*., 2013] and +0.2‰ for *C. pelagicus* [*Ziveri et al*., 2003].

[b]The species *C. pelagicus* and *C. leptoporus* dominate the NF fraction, the other constituents (Other) account for only 10% in average of the fraction and consist mainly in *Discoaster* spp. and *S. abies* for which the oxygen isotopic biologic fractionations are unknown. Because of their low contribution they have been neglected in the calculation of $\delta^{18}O_{NF\ eq}$.

4.3. Stable Isotope Results

The planktic foraminifera species *D. venezuelana* and the NF fraction yield parallel $\delta^{18}O$ and $\delta^{13}C$ evolutions (Figures 3b and 3d). The NF fraction records the highest isotopic amplitude variability throughout the studied interval, especially for $\delta^{13}C$ (Figure 3d).

During unit A, $\delta^{18}O$ of NF and the *G. menardii* decrease by 0.5‰ and *D. venezuelana* by 0.8‰. The $\delta^{18}O$ and $\delta^{13}C$ of all records increase significantly during unit B (1‰ for NF and 0.5‰ for *G. menardii* and *D. venezuelana*), reaching maximum values at the beginning of the unit C (~ 177.5 m). While $\delta^{18}O$ remain generally high until the end of unit C, $\delta^{13}C$ drop to lower values from 177.5 m to 177 m (by 1‰ for NF and ~0.4‰ for both foraminifera). During unit D, $\delta^{18}O$ continuously decrease, reaching minimum values at the end of this unit and remain stable and low until the end of the studied interval.

The NF fraction displays systematically lighter $\delta^{18}O$ and $\delta^{13}C$ values compared to *D. venezuelana* and *G. menardii*, with $\delta^{18}O$ values ranging from −0.97‰ to 0.06‰ and $\delta^{13}C$ varying between −0.05‰ and 1.27‰ (Table 2 and Figures 3b and 3d). *G. menardii* has the most positive $\delta^{13}C$ (between 1.27‰ and 2.16‰), while *D. venezuelana* show intermediate values ranging from 0.69‰ to 1.85‰.

During unit C, *G. menardii* yield the most positive $\delta^{18}O$ values, whereas in the other units, $\delta^{18}O_{G.\ menardii}$ are intermediate between NF and *D. venezuelana*, $\delta^{18}O_{D.\ venezuelana}$ being slightly more positive than $\delta^{18}O_{G.\ menardii}$ (Figure 3b).

5. Discussion

5.1. Biogenic Carbonate Supply

The strong correlation between the total number of nannofossils and small *Dictyococcites* spp. ($R^2 = 0.95$) and the low variability of the minor taxa indicate that calcareous nannofossil production has been dominated by this single species for almost 100 kyr.

The correlation between $CaCO_3$ and the number of nannofossils (Figures 2a and 2c) observed in units B and C indicates that there is an increase of carbonate burial due to the increase of small *Dictyococcites* spp. However,

during unit A and from unit D and thereafter, the total number of calcareous nannofossil decreases, while the carbonate content remains high (around 80%), reflecting a shift in the carbonate source before and after unit C.

The Cenozoic ancestors of *Gephyrocapsa oceanica* and *E. huxleyi* evolved from the *Reticulofenestra*/*Dictyococcites* plexus [*Marlowe et al*., 1990; *Young et al*., 1992; *Henderiks and Pagani*, 2008], it is thus likely that the members of the *Reticulofenestra-Dictyococcites-Gephyrocapsa-Emiliania* lineage have had similar ecological preferences. Modern *E. huxleyi* and *Gephyrocapsa* spp. are cosmopolitan species with a wide environmental tolerance [*Rickaby et al*., 2007], both species being able to grow rapidly and form large blooms [*Bollmann et al*., 1998; *Wang et al*., 2003] out competing other species at high light levels [*Nanninga and Tyrrell*, 1996]. By analogy, the small *Dictyococcites* spp. may have been able to take advantage of the changing environmental conditions thereby out competing other species—resulting in a significant increase in biogenic carbonate burial.

To investigate the causes of their sudden dominance in the total carbonate production in unit C, we reconstructed environmental conditions of the upper water column.

5.2. Stable Isotope Record and Upper Water Column Structure

5.2.1. Depth Distribution of the Foraminifera Species

$\delta^{18}O$ and $\delta^{13}C$ of planktic foraminifera species *G. menardii* and *D. venezuelana* were used to assess properties of the upper water column. *G. menardii* is believed to calcify in the upper thermocline (100–200 m) [*Schweitzer and Lohmann*, 1991], possibly depth migrating with the chlorophyll maximum zone [*Fairbanks et al*., 1980; *Watkins et al*., 1998], but the depth habitat of *D. venezuelana* is still open to discussion. *Stewart et al*. [2012] suggested that the latter species might have shifted its calcification depth from the mixed layer, to the thermocline (from late Oligocene to early Miocene) and to the subthermocline waters (from mid-Miocene to younger age). Here we evaluate the calcification depth of *D. venezuelana*, by comparison with the NF fraction taken as the isotopic reference for the mixed layer where the calcareous nannofossils calcify [*Okada and Honjo*, 1973].

Assuming that the more positive carbonate $\delta^{18}O$ values are found in deeper waters (because of decreasing temperature and increasing salinity, $\delta^{18}O_w$), the observed isotopic offset between the NF fraction and the upper thermocline dweller *G. menardii* is consistent with their respective depth habitats. The $\delta^{18}O$ of *D. venezuelana* lying between NF and *G. menardii* (Figure 3b) suggests a calcification depth between the mixed layer and the upper thermocline. Unlike $\delta^{18}O$, the carbonate $\delta^{13}C$ decreases with depth. This essentially reflects the fact that phytoplankton preferentially use $^{12}CO_2$ during photosynthesis which thus increase the $\delta^{13}C_{DIC}$ and that heterotrophic organisms reintroduce $^{12}CO_2$ back into the Dissolved Inorganic Carbon (DIC) pool at depth via respiration [*Kroopnick*, 1974]. However, as shown in Figure 3d, NF records the lightest $\delta^{13}C$ which conflicts with the relative bathymetric distribution of coccoliths and *G. menardii*.

Several parameters influence the isotopic composition of biogenic calcite among which species-specific vital effects. Modern coccoliths are known to exhibit a nearly 5‰ array of interspecific vital effects in $\delta^{18}O$ [*Dudley and Goodney*, 1979; *Dudley et al*., 1986] and $\delta^{13}C$ [*Ziveri et al*., 2003; *Rickaby et al*., 2010]. Isotopic disequilibrium is also observed for several species of planktic foraminifera [*Spero and Lea*, 1996; *Bemis et al*., 2000].

Vital effects ($\delta^{13}C$) are related to a series of complex physiological factors such as photosymbionts, respiration and carbonate ion concentrations for foraminifera [*Mulitza et al*., 1997], photosynthesis rates, and cell sizes for coccolithophores [*Ziveri et al*., 2003; *Rickaby et al*., 2010; *Bolton et al*., 2012; *Bolton and Stoll*, 2013]. Because the carbon isotope vital effects are still poorly constrained, we will only correct for the vital effect on the $\delta^{18}O$.

The use of polyspecific NF fractions raises the problem of whether the relative contribution of different species with different vital effects could partially overwhelm or bias the isotopic signals [*Stoll*, 2005]. *Ziveri et al*. [2003] proposed a correction of +0.2‰ on the $\delta^{18}O$ of *C. pelagicus* based on culture experiments that was confirmed by recent studies showing that this species calcifies close to equilibrium [*Stevenson et al*., 2014]. Additionally, *Candelier et al*. [2013] found a -1.1‰ offset from equilibrium calcite in modern *C. leptoporus*.

Although little is known about vital effects through geological times, recent study by *Bolton and Stoll* [2013] suggests that the large oxygen and carbon vital effects ($>$ 1‰) recorded in modern coccoliths appeared only during the latest Miocene. As the vital effect corrections proposed by *Candelier et al*. [2013] and *Ziveri et al*. [2003] for *C. pelagicus* and *C. leptoporus* are close or under 1‰, we believe that they are consistent with the *Bolton and Stoll* [2013] model. Using these estimates and the relative proportion of these two calcareous nannofossil species in the separated fractions, we applied a vital effect correction on the $\delta^{18}O_{NF}$ (Table 2 and

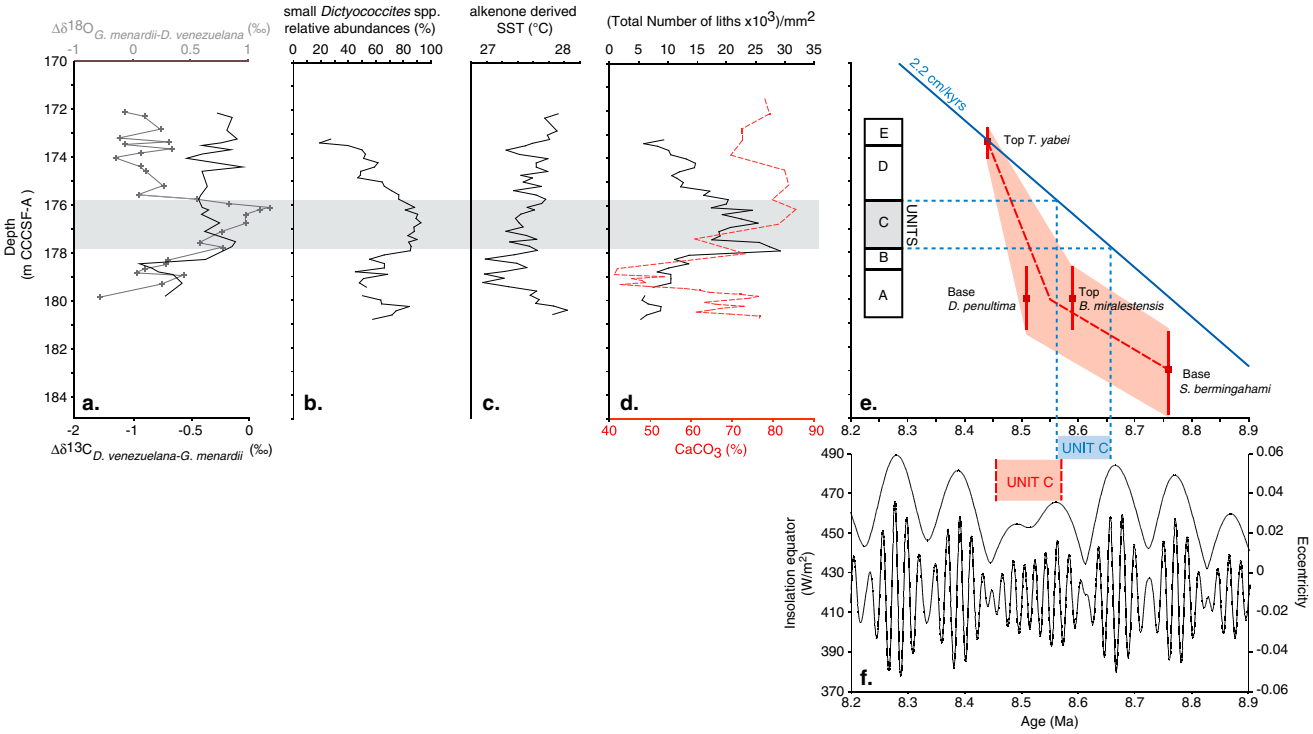

Figure 4. Main results of our study compared with eccentricity and insolation at the equator. (a) Oxygen and carbon isotopic gradients between upper thermocline and mixed-layer species *G. menardii* and *D. venezuelana*, (b) small *Dictyococcites* spp. relative abundance in the calcareous nannofossil assemblage (c) alkenone-derived SSTs, and (d) total number of calcareous nannofossils per mm^2 and $CaCO_3$ variations for Site U1338. (e) The linear age model for the intervals 157.3 m and 201.2 m for Site U1338 (blue line) and the main biostratigraphic datum and their depth error (red bars) found in the present study interval (see Table 1). (f) The orbital insolation at the equator and eccentricity sequences for the studied interval are shown [*Laskar et al.*, 2004]. When using the linear age model (blue line), the studied interval is dated between 8.81 and 8.39 Ma, and unit C corresponds to a node in insolation at the equator under low eccentricity (grey-shaded interval in Figure 4f); however, the onset of the acme (unit B) coincides with a peak in insolation. When using the biostratigraphic datum, which provides more robust age control (red-shaded area), unit C is shifted toward younger age and falls in the interval of low-insolation and eccentricity variations where unit B, the initiation of the acme, coincides with a node in insolation.

Figure 3c). Finally, although nonspinose planktic foraminifera are considered to have limited vital effects [*Fairbanks et al.*, 1980, 1982], we also applied a correction of +0.3‰ on the $\delta^{18}O$ values of *G. menardii*, as suggested by *Bouvier-Soumagnac and Duplessy* [1985] (Figure 3c).

Vital effects corrected $\delta^{18}O$ of NF ($\delta^{18}O_{NFeq}$) and *G. menardii* ($\delta^{18}O_{G.menardii\ eq}$) are still consistent with their relative water depth distribution, with $\delta^{18}O$ varying from 0.13‰ to 0.65‰ and from −0.3‰ to 1.1‰, respectively (Figure 3c). Regarding *D. venezuelana*, our $\delta^{18}O$ data indicate that specimens from 300 to 355 μm size fraction calcified exclusively in the mixed layer, in agreement with $\delta^{18}O_{NFeq}$. Based on these observations, we suggest that *D. venezuelana* (300–355 μm) was a mixed-layer dweller during the late Miocene. Our data are at odds with previous studies suggesting migration of *D. venezuelana* to subthermocline waters during the mid-Miocene [*Stewart et al.*, 2012, and references therein]. We postulate the smaller <355 μm individuals are mixed-layer dwellers throughout their range and that larger (adult) specimens of *D. venezuelana* migrate through the water column and that this migration through ontogeny has been a feature throughout their lineage.

5.2.2. Upper Water Column Structure

The $\delta^{18}O$ of planktic and benthic foraminifera display similar long-term trends between 10 Ma and 7 Ma [*Rousselle et al.*, 2013] interpreted as reflecting the Antarctic ice sheet volume. Changes of the upper water column stratification were estimated from the difference between the isotopic values of the mixed-layer foraminifera species *D. venezuelana* and upper thermocline dweller *G. menardii* after removing the global ice volume effect. Oxygen gradient ($\Delta\delta^{18}O_{G.menardii\text{-}D.venezuelana}$) variations gauge the thermocline depth changes [*Mulitza et al.*, 1997], while the carbon isotopic gradients ($\Delta\delta^{13}C_{D.venezuelana\ -G.menardii}$) provide some hints into the surface water nutrient profile [*Nathan and Leckie*, 2009]. The shoaling of the thermocline and the nutricline leads to an increase of the $\delta^{18}O$ gradient and a reduced $\delta^{13}C$ gradient between the upper thermocline and mixed layer.

The $\Delta\delta^{18}O_{G.\ menardii\text{-}D.\ venezuelana}$ gradient (Figure 4a) shows a broad increase from 178.47 m to 176.10 m of ~1‰ covering half of unit B and unit C. From 176.10 m to 175.5 m, values drastically decrease by the same amount at the onset of unit D and remained relatively stable and low until 172.2 m. Those fluctuations of the $\delta^{18}O$ gradient indicate a deep thermocline during units A, B, D, and E, shoaling to its shallowest position at the very end of unit C, around 176.10 m (Figure 4a).

According to the relative depth distribution of *D. venezuelana* (mixed layer) and *G. menardii* (upper thermocline), we would expect the $\Delta\delta^{13}C_{\ D.venezuelana\text{-}G.menardii}$ to be positive (Figure 4a), while we observe negative values varying between −0.94 and −0.06‰. An interspecific $\delta^{13}C$ vital effect is the most likely explanation for this discrepancy. The $\delta^{13}C$ offsets from equilibrium are unknown for *D. venezuelana* and *G. menardii*. However, based on our $\Delta\delta^{13}C$ gradient values, we suggest the minimum $\delta^{13}C$ interspecific vital effect correction should be around +1‰, which is in agreement with studies of modern foraminifera cultures and plankton tows [e.g., *Spero et al*., 2003; *Bemis et al*., 2000; *Ortiz et al*., 1996]. As a consequence, we interpret only the trends of the uncorrected $\Delta\delta^{13}C_{\ D.venezuelana\ \text{-}G.menardii}$.

Figure 4a shows that the $\delta^{13}C$ and $\delta^{18}O$ gradients either yield parallel trends (units A and B) or do not correlate (units C and D), indicating that the thermocline and nutricline depths evolved independently throughout the interval studied.

Different scenarios could explain the observed nutricline and thermocline behavior:

According to *Cannariato and Ravelo* [1997], change in the nutrient regeneration depth or a stronger seasonality in surface nutrient concentrations could account for such $\Delta\delta^{13}C$ changes. In this latter case, this would imply that *G. menardii* and *D. venezuelana* calcified at different seasons. *Nathan and Leckie* [2009] hypothesize enhanced seasonality based on foraminifera species diversity changes, at 8.6 Ma in the western equatorial Pacific Ocean Drilling Program (ODP) Site 806. However, this information is not available at Site U1338.

Alternatively, foraminifera depth migration could also be the cause of the observed oxygen and carbon isotopic gradients between the mixed layer and the thermocline. Based on the similarity between *D. venezuelana* and the NF_{eq} isotopic variation amplitudes (Figure 3c), it is unlikely that *D. venezuelana* in the 300–355 μm size fraction migrated out of the mixed layer. However, *Fairbanks et al*. [1980] and *Watkins et al*. [1998] mention that the depth distribution of *G. menardii* is tightly coupled to the depth of the chlorophyll maximum. In the modern ocean, the $\delta^{13}C_{DIC}$, temperature, and salinity gradients within the upper pycnocline are steep [*Fairbanks et al*., 1982], a small downward migration of *G. menardii* in the upper thermocline could significantly increase both the $\delta^{13}C$ and $\delta^{18}O$ gradients. Either hypothesis is difficult to assess with our data set. However, some lines of evidence tend to favor the depth migration of *G. menardii*.

First, as mentioned previously, during units B and C the carbonate production is dominated by the small *Dictyococcites* spp. This high primary production in unit C, together with a shallow thermocline should have favored high abundances of *G. menardii* [*Thunell and Reynolds*, 1984; *Martinez et al*., 1998; *Andreasen and Ravelo*, 1997]. However, although no foraminifera counts were performed for this study, well-preserved *G. menardii* were present in unit C but in very low abundances.

Second, the depth shifts of the thermocline derived from the $\Delta\delta^{18}O$ are not supported by alkenone SSTs that indicate warm and stable conditions (Figure 4c). This suggests that the thermocline shoaling during unit C did not influence the mixed-layer temperatures, which is in agreement with *La Riviere et al*. [2012]. According to these authors, during the Miocene, the equatorial Pacific thermocline was deep and homogenous as also suggested by the long-term alkenone-derived SST record for Site U1338, indicating continuous stable and warm surface temperatures between ~12 and 7 Ma [*Rousselle et al*., 2013].

Altogether, the stable and warm SSTs, the deep thermocline, and the decrease of *G. menardii* abundances in unit C indicate that the observed oxygen and carbon isotopic gradients are biased by the depth migration of *G. menardii* that artificially enhance the amplitude of the thermocline and nutricline vertical variations.

5.3. Late Miocene Small *Dictyococcites* spp. Acme: Local or Global Environmental Control?

Based on our reconstruction of environmental conditions, the surface ocean stratification fails to explain the small *Dictyococcites* spp. dominance. Our results indicate that the acme occurred in warm surface waters, with low nutrient supply as the thermocline remained deep. The success of small *Dictyococcites* spp. at Site U1338 may thus be related to external forcing.

Studies on more recent coccolithophore acmes provide several hypothesis which may explain this late Miocene small *Dictyococcites* spp. acme, among which the "Silica Leakage Hypothesis" from the Southern Ocean and the orbital control on the opportunistic coccolithophores [*Rickaby et al*., 2007]. Because of limited interactions between the thermocline and the mixed layer where small *Dictyococcites* spp. develop, the "Silica Leakage Hypothesis" does not adequately explain the observed calcareous nannofossil production increase (Figures 2 and 4).

The benthic foraminifera δ^{18}O decrease (~0.4‰ ODP Site 1085) [*Westerhold et al*., 2005] around 8.5 Ma and evidences for successive subglacial meltwater discharges from the East Antarctic Ice Sheet in the Ross Sea area, between 9 and 8 Ma [*McKay et al*., 2009], point to reduced ice volume. According to *Koutavas et al*. [2002], under such conditions calcareous phytoplankton production dominate because of lower silica leakage from the Southern Ocean. The resulting Si-depleted waters might have fed the EUC, but since we do not observe a shoaling of the thermocline in the EEP as also found by *La Riviere et al*. [2012], high-latitude control of the equatorial productivity can be ruled out. In that context, we suggest that light intensity likely played the most important role in the small *Dictyococcites* spp. dominance at Site U1338.

Rickaby et al. [2007] proposed that coccolithophore acme events might be related to eccentricity through its influence on light intensity and coccolithophore growing season length. We cannot conclusively test this hypothesis because our age model relies on biostratigraphic age control with inherent depth errors (see section 3.3 and Figure 4), which prevents us from accurate comparison with the orbital timescale. However, regardless of the depth and timing errors, the onset and peak of small *Dictyococcites* spp. production coincides with a period of low-eccentricity variability [*Laskar et al*., 2004]. We speculate, that the match between the low-eccentricity interval and the small *Dictyococcites* spp. acme agrees with the hypothesis made by *Rickaby et al*. [2007] for the Pleistocene *E. huxleyi* and *G. caribbeanica* acmes. These authors interpreted such events as reflecting the adaptation response of opportunistic species to stable insolation conditions during low-eccentricity interval [*Richmond et al*., 2005]. Whether this orbital theory may stand by itself to explain the success of the late Miocene small *Dictyococcites* spp. acme remains an open question.

6. Conclusions

Our multiproxy geochemical study sheds new light on sea surface conditions of the EEP during the late Miocene small *Dictyococcites* spp. acme. Our data indicate that the EEP thermocline was deep and stable during the acme period, around 8.6 Ma, in agreement with previous results from *La Riviere et al*. [2012]. We also show that the small *Dictyococcites* spp. production and dominance were likely independent of SSTs. Our reconstruction of the surface conditions of the EEP does not support the idea of a Southern Ocean control of nutrient supply during this interval. Instead, we speculate that this acme would, in part, be caused by low-eccentricity and low-insolation variability at the equator, favoring the dominance of potentially high light intensity adapted species according to the hypothesis put forward by *Rickaby et al*. [2007] for Pleistocene *E. huxleyi* and *G. caribbeanica* acmes.

Acknowledgments
This research used samples and data provided by the Integrated Ocean Drilling Program (IODP). Funding for this work was provided by grants from the INSU 2010 ACTION COORDONNEE "Campagne à la mer". We would like to thank Nathalie Labourdette (Laboratoire Biominéralisations et Environnements sédimentaires, ISTeP - UPMC) for technical support with isotope analyses. We thank the Expedition 320/321 staff and Shipboard Scientific Party, and the JOIDES Resolution crew for their efforts in collecting the core upon which this study is based. We sincerely thank J. Henderiks and the anonymous reviewers for helpful comments and constructive criticisms that greatly improved the manuscript.

References

Andreasen, D. J., and A. C. Ravelo (1997), Tropical Pacific Ocean thermocline depth reconstructions for the last glacial maximum, *Paleoceanography*, *12*, 395–413, doi:10.1029/97PA00822.

Aubry, M. P. (1992), Paleogene calcareous nannofossils from the Kerguelen Plateau, Leg 120, in *Proc. ODP Sci. Results*, vol. 120, edited by S. W. Wise Jr. et al., pp. 471–491, College Station, Tex.

Backman, J. (1980), Miocene-Pliocene nannofossils and sedimentation rates in the Hatton-Rockall Basin, NE Atlantic Ocean, *Stockholm Contrib. Geol.*, *36*, 1–91.

Backman, J., and N. J. Shackleton (1983), Quantitative biochronology of Pliocene and Pleistocene calcareous nannofossils from the Atlantic, Indian and Pacific Oceans, *Mar. Micropaleontol.*, *8*, 141–170.

Backman, J., I. Raffi, M. Ciummelli, and J. Baldauf (2013), Species-specific responses of late Miocene *Discoaster* spp. to enhanced biosilica productivity conditions in the equatorial Pacific and the Mediterranean, *Geo Mar. Lett.*, *33*, 285–298, doi:10.1007/s00367-013-0328-0.

Beaufort, L. (1992), Dynamique du nannoplancton calcaire au cours du Néogène: Implications climatiques et océanographiques, *Doc. Lab. Géol. Lyon*, *121*, 1–141.

Bemis, B. E., H. J. Spero, D. W. Lea, and J. Bijma (2000), Temperature influence on the carbon isotopic composition of *Globigerina bulloides* and *Orbulina universa* (planktonic foraminifera), *Mar. Micropaleontol.*, *38*, 213–228.

Bollmann, J., K. H. Baumann, and H. R. Thierstein (1998), Global dominance of *Gephyrocapsa* coccoliths in the late Pleistocene: Selective dissolution, evolution, or global environmental change?, *Paleoceanography*, *13*, 517–529.

Bolton, C. T., and H. M. Stoll (2013), Late Miocene threshold response of marine algae to carbon dioxide limitation, *Nature*, *500*, 558–562, doi:10.1038/nature12448.

Bolton, C. T., H. M. Stoll, and A. Mendez Vicente (2012), Vital effects in coccolith calcite: Cenozoic climate-P_{CO2} drove the diversity of carbon acquisition strategies in coccolithophores?, *Paleoceanography*, *27*, PA4204, doi:10.1029/2012PA002339.

Bouvier-Soumagnac, Y., and J.-C. Duplessy (1985), Carbon and oxygen isotopic composition of planktonic foraminifera from laboratory culture, plankton tows and recent sediment: Implications for the reconstruction of paleoclimatic conditions and of the global carbon cycle, *J. Foraminiferal Res.*, *15*, 302–320.

Brown, C. W., and J. A. Yoder (1994), Coccolithophorid blooms in the global ocean, *J. Geophys. Res.*, *99*, 7467–7482.

Candelier, Y., F. Minoletti, I. Probert, and M. Hermoso (2013), Temperature dependence of oxygen isotope fractionation in coccolith calcite: A culture and core top calibration of the genus *Calcidiscus*, *Geochim. Cosmochim. Acta*, *100*, 264–281, doi:10.1016/j.gca.2012.09.040.

Cannariato, K. G., and A. C. Ravelo (1997), Pliocene-Pleistocene evolution of eastern tropical Pacific surface water circulation and thermocline depth, *Paleoceanography*, *12*, 805–820.

Conte, M. H., M.-A. Sicre, C. Rühlemann, J. C. Weber, S. Schulte, D. Schulz-Bull, and T. Blanz (2006), Global temperature calibration of the alkenone unsaturation index ($U^{k'}_{37}$) in surface waters and comparison with surface sediments, *Geochem. Geophys. Geosyst.*, *7*, Q02005, doi:10.1029/2005GC001054.

Deser, C., and J. M. Wallace (1990), Large-scale atmospheric circulation features of warm and cold episodes in the tropical Pacific, *J. Clim.*, *3*, 1254–1282.

Dudley, W. C., and D. E. Goodney (1979), Oxygen isotope analyses of coccoliths grown in culture, *Deep Sea Res., Part A*, *26*, 495–503.

Dudley, W. C., P. Blackwelder, L. Brand, and J. C. Duplessy (1986), Stable isotopic composition of coccoliths, *Mar. Micropaleontol.*, *10*, 1–8.

Egge, J. K., and D. L. Aksnes (1992), Silicate as a regulating nutrient in phytoplankton competition, *Mar. Ecol. Prog. Ser.*, *83*, 281–289.

Fairbanks, R. G., P. H. Wiebe, and A. W. Bé (1980), Vertical distribution and isotopic composition of living planktonic foraminifera in the western North Atlantic, *Science*, *207*, 61–63.

Fairbanks, R. G., M. Sverdlove, R. Free, P. H. Wiebe, and A. W. Bé (1982), Vertical distribution and isotopic fractionation of living planktonic foraminifera from the Panama Basin, *Nature*, *298*, 841–844.

Flores, J. A., F. J. Sierro, and I. Raffi (1995), Evolution of the calcareous nannofossil assemblage as a response to the paleoceanographic changes in the eastern equatorial Pacific ocean from 4 to 2 Ma (Leg 138, Sites 849 and 852), in *Proc. ODP Sci. Results*, vol. 138, edited by N. G. Pisias et al., pp. 163–176, College Station, Tex.

Flower, B. P., and J. P. Kennett (1994), The middle Miocene climatic transition: East Antarctic ice sheet development, deep ocean circulation and global carbon cycling, *Palaeogeogr. Palaeoclimatol. Palaeoecol.*, *108*, 537–555.

Foster, G. L., C. H. Lear, and J. W. B. Rae (2012), The evolution of pCO_2, ice volume and climate during the middle Miocene, *Earth Planet. Sci. Lett.*, *341-344*, 243–254.

Fox, L. R., and B. S. Wade (2013), Systematic taxonomy of early–middle Miocene planktonic foraminifera from the equatorial Pacific Ocean: Integrated Ocean Drilling Program, Site U1338, *J. Foraminiferal Res.*, *43*, 373–404.

Franck, V. M., M. A. Brzezinsky, K. Coale, and D. Nelson (2000), Iron and silicic acid availability regulate Si uptake in the Pacific sector of the Southern Ocean, *Deep Sea Res., Part II*, *47*, 3315–3338.

Gartner, S. (1988), Paleoceanography of the mid-Pleistocene, *Mar. Micropaleontol.*, *13*, 23–46.

Hayashi, H., K. Idemitsu, B. S. Wade, Y. Idehara, K. Kimoto, H. Nishi, and H. Matsui (2013), Middle Miocene to Pleistocene planktonic foraminiferal biostratigraphy in the eastern equatorial Pacific Ocean, *Paleontol. Res.*, *17*, 91–109.

Henderiks, J. (2008), Coccolithophore size rules—Reconstructing ancient cell geometry and cellular calcite quota from fossil coccoliths, *Mar. Micropaleontol.*, *67*, 143–154.

Henderiks, J., and M. Pagani (2007), Refining ancient carbon dioxide estimates: Significance of coccolithophore cell size for alkenone-based pCO_2 records, *Paleoceanography*, *22*, PA3202, doi:10.1029/2006PA001399.

Henderiks, J., and M. Pagani (2008), Coccolithophore cell size and the Paleogene decline in atmospheric CO_2, *Earth Planet. Sci. Lett.*, *269*, 576–584.

Kameo, K., and T. J. Bralower (2000), Neogene calcareous nannofossil biostratigraphy of Sites 998, 999, and 1000, Caribbean Sea, in *Proceedings of the Ocean Drilling Program*, Scientific Results, vol. 165, edited by R. M. Leckie et al., pp. 3–18, Ocean Drilling Program, College Station, Tex.

Kamikuri, S., I. Motoyama, H. Nishi, and M. Iwai (2009), Evolution of eastern Pacific warm pool and upwelling processes since the middle Miocene based on analysis of radiolarian assemblages: Response to Indonesian and Central American seaways, *Palaeogeogr. Palaeoclimatol. Palaeoecol.*, *280*, 469–479.

Koutavas, A., J. Lynch-Stieglitz, T. M. Marchitto Jr., and J. P. Sachs (2002), El Niño-like pattern in ice age tropical Pacific sea surface temperature, *Science*, *297*, 226–230, doi:10.1126/science.1072376.

Kroopnick, P. (1974), The dissolved O_2-CO_2-^{13}C system in the eastern equatorial Pacific, *Deep Sea Res.*, *32*, 57–84.

La Riviere, J. P., A. C. Ravelo, A. Crimmins, P. S. Dekens, H. L. Ford, M. Lyle, and M. W. Wara (2012), Late Miocene decoupling of oceanic warmth and atmospheric carbon dioxide forcing, *Nature*, *486*, 97–100, doi:10.1038/nature11200.

Laskar, J., P. Robutel, F. Joutel, M. Gastineau, A. C. M. Correia, and B. Levrard (2004), A long term numerical solution for the insolation quantities of the Earth, *Astron. Astrophys.*, *428*, 261–285, doi:10.1051/0004-6361:20041335.

Levitus, S., and T. P. Boyer (1994), *World Ocean Atlas 1994*, Temperature, NOAA Atlas NESDIS, vol. 4, 129 pp., U.S. Dept. of commerce, Washington, D. C.

Loubere, P. (2000), Marine control of biological production in the eastern equatorial Pacific Ocean, *Nature*, *406*, 497–500, doi:10.1038/35020041.

Lyle, M., and J. Backman (2013), Data report: Calibration of XRF-estimated $CaCO_3$ along the Site U1338 splice, in *Proc. IODP*, vol. 320/321, edited by H. Pälike et al., and the Expedition 320/321 Scientists, 16 pp., Tokyo, doi:10.2204/iodp.proc.320321.205.2013.

Marlowe, I. T., S. C. Brassell, G. Eglinton, and J. C. Green (1990), Long-chain alkenones and alkyl alkenoates and the fossil coccolith record of marine sediments, *Chem. Geol.*, *88*, 349–375.

Martinez, J., L. Taylor, P. Deckker, and T. Barrows (1998), Planktonic foraminifera from the eastern Indian Ocean: Distribution and ecology in relation to the western Pacific warm pool (WPWP), *Mar. Micropaleontol.*, *34*, 121–151.

Matsumoto, K., J. L. Sarmiento, and M. A. Brzezinski (2002), Silicic acid leakage from the Southern Ocean: A possible explanation for glacial atmospheric pCO_2, *Global Biogeochem. Cycles*, *16*(3), 1031, doi:10.1029/2001GB001442.

McKay, R., et al. (2009), The stratigraphic signature of the late Cenozoic Antarctic ice sheets in the Ross embayment, *Geol. Soc. Am. Bull.*, *121*(11–12), 1537–1561, doi:10.1130/B26540.1.

Minoletti, F., M. Hermoso, and V. Gressier (2009), Separation of sedimentary micron-sized particles for palaeoceanography and calcareous nannoplankton biogeochemistry, *Nat. Protoc.*, *4*, 14–24, doi:10.1038/nprot.2008.200.

Mulitza, S., A. Dürkoop, W. Hale, G. Wefer, and H. S. Niebler (1997), Planktonic foraminifera as recorders of past surface-water stratification, *Geology*, *25*, 335–338, doi:10.1130/0091-7613.

Nanninga, H. J., and T. Tyrrell (1996), Importance of light for the formation of algal blooms by *Emiliania huxleyi*, *Mar. Ecol. Prog. Ser.*, *136*, 195–203, doi:10.3354/meps136195.

Nathan, S. A., and R. M. Leckie (2009), Early history of the western Pacific warm pool during the middle to late Miocene (~13.2–5.8 Ma): Role of sea-level change and implications for equatorial circulation, *Palaeogeogr. Palaeoclimatol. Palaeoecol.*, *274*, 140–159.
Okada, H., and S. Honjo (1973), The distribution of oceanic coccolithophorids in the Pacific, *Deep Sea Res., Part A*, *20*, 355–374.
Ortiz, J. D., A. C. Mix, W. Rugh, J. M. Watkins, and R. W. Collier (1996), Deep-dwelling planktonic foraminifera of the northeastern Pacific Ocean reveal environmental control of oxygen and carbon isotope disequilibria, *Geochim. Cosmochim. Acta*, *60*, 4509–4523.
Pagani, P., J. C. Zachos, K. H. Freeman, B. Tipple, and S. Bohaty (2005), Marked decline in atmospheric carbon dioxide concentrations during the Paleogene, *Science*, *309*, 600–603, doi:10.1126/science.1110063.
Paillard, D., L. Labeyrie, and P. Yiou (1996), Macintosh program performs time-series analysis, *Eos Trans. AGU*, *77*, 379.
Pälike, H., M. Lyle, H. Nishi, I. Raffi, K. Gamage, A. Klaus, and the Expedition 320/321 Scientists (2010), *Proc. IODP*, vol. 320/321, Integrated Ocean Drilling Program Management International, Inc., Tokyo, doi:10.2204/iodp.proc.320321.2010.
Pearson, P. N., and M. R. Palmer (2000), Atmospheric carbon dioxide concentrations over the past 60 million years, *Nature*, *406*, 695–699, doi:10.1038/35021000.
Philander, S. G. H. (1980), The equatorial undercurrent revisited, *Annu. Rev. Earth Planet. Sci.*, *8*, 191–204.
Plancq, J., V. Grossi, J. Henderiks, L. Simon, and E. Mattioli (2012), Alkenone producers during late Oligocene–early Miocene revisited, *Paleoceanography*, *27*, PA1202, doi:10.1029/2011PA002164.
Prahl, F. G., L. A. Muehlhausen, and D. L. Zahnle (1988), Further evaluation of long-chain alkenones as indicators of paleoceanographic conditions, *Geochim. Cosmochim. Acta*, *52*, 2303–2310.
Richmond, C. E., D. L. Breitburg, and K. A. Rose (2005), The role of environmental generalist species in ecosystem function, *Ecol. Modell.*, *188*, 279–295.
Rickaby, R. E. M., E. Bard, C. Sonzogni, F. Rostek, L. Beaufort, S. Barker, G. Rees, and D. P. Schrag (2007), Coccolith chemistry reveals secular variations in the global ocean carbon cycle?, *Earth Planet. Sci. Lett.*, *253*, 83–95.
Rickaby, R. E. M., J. Henderiks, and J. N. Young (2010), Perturbing phytoplankton: Response and isotopic fractionation with changing carbonate chemistry in two coccolithophore species, *Clim. Past*, *6*, 771–785.
Rio, D., E. Fornaciari, and I. Raffi (1990), Late Oligocene through early Pleistocene calcareous nannofossils from western equatorial Indian Ocean (Leg 115), in *Proc. ODP, Sci. Results*, vol. 115, edited by R. A. Duncan et al., pp. 175–235, College Station, Tex.
Rousselle, G., C. Beltran, M.-A. Sicre, I. Raffi, and M. De Rafélis (2013), Changes in sea-surface conditions in the Equatorial Pacific during the middle Miocene-Pliocene as inferred from coccolith geochemistry, *Earth Planet. Sci. Lett.*, *361*, 412–421.
Schweitzer, P. N., and G. P. Lohmann (1991), Ontogeny and habitat of modern menardii form planktonic foraminifera, *J. Foraminiferal Res.*, *21*, 332–346.
Sicre, M.-A., Y. Ternois, M. Paterne, P. Martinez, and P. Bertrand (2001), Climatic changes in the upwelling region off Cap Blanc, NW Africa, over the last 70 kyrs, a multi-biomarker approach, *Org. Geochem.*, *32*, 981–990.
Spero, H. J., and D. W. Lea (1996), Experimental determination of stable isotope variability in *Globigerina bulloides*: Implications for paleoceanographic reconstructions, *Mar. Micropaleontol.*, *28*, 231–246.
Spero, H. J., K. M. Mielke, E. M. Kalve, D. W. Lea, and D. K. Pak (2003), Multi-species approach to reconstructing eastern equatorial Pacific thermocline hydrography during the past 360 ky, *Paleoceanography*, *18*(1), 1022, doi:10.1029/2002PA000814.
Stevenson, E. I., M. Hermoso, R. E. M. Rickaby, J. J. Tyler, F. Minoletti, I. J. Parkinson, F. Mokadem, and K. W. Burton (2014), Controls on Stable strontium isotope fractionation in coccolithophores with implications for the marine Sr cycle, in *Geochim. Cosmochim. Acta*, *128*, 225–235, doi:10.1016/gca.2013.11.043.
Stewart, J. A., P. A. Wilson, K. M. Edgar, P. Anand, and R. H. James (2012), Geochemical assessment of the palaeoecology, ontogeny, morphotypic variability and palaeoceanographic utility of "*Dentoglobigerina*" *venezuelana*, *Mar. Micropaleontol.*, *84-85*, 74–86.
Stewart, R. H. (2005), *Introduction to Physical Oceanography*, Department of Oceanography, Texas A and M University, Open source textbook. [Available at http://oceanworld.tamu.edu/resources/ocng_textbook/contents.html.]
Stoll, H. M. (2005), Limited range of interspecific vital effects in coccolith stable isotopic records during the Paleocene-Eocene thermal maximum, *Paleoceanography*, *20*, PA1007, doi:10.1029/2004PA001046.
Takayama, T. (1993), Notes on Neogene calcareous nannofossil biostratigraphy of the Ontong Java Plateau and size variations of Reticulofenestra coccoliths, in *Proceedings of the Ocean Drilling Program*, Scientific Results, vol. 130, edited by W. H. Berger, L. W. Kroenke, and L. A. Mayer, pp. 179–230, Ocean Drilling Program, College Station, Tex.
Thunell, R. C., and L. A. Reynolds (1984), Sedimentation of planktonic foraminifera: Seasonal changes in species flux in the Panama Basin, *Micropaleontology*, *30*(243), 262.
Toggweiler, J. R., K. Dixon, and W. S. Broecker (1991), The Peru upwelling and the ventilation of the South Pacific thermocline, *J. Geophys. Res.*, *96*, 20,467–20,497.
Wade, B. S., W. A. Berggren, and R. K. Olsson (2007), The biostratigraphy and paleobiology of Oligocene planktonic foraminifera from the equatorial Pacific Ocean (ODP Site 1218), *Mar. Micropaleontol.*, *62*, 167–179.
Wang, P., J. Tian, X. Cheng, C. Liu, and J. Xu (2003), Carbon reservoir change preceded major ice-sheet expansion at the mid-Brunhes event, *Geology*, *31*, 239–242.
Watkins, J. W., A. C. Mix, and J. Wilson (1998), Living planktic foraminifera in the central tropical Pacific Ocean: Articulating the equatorial "Cold Tongue" during La Nina, 1992, *Mar. Micropaleontol.*, *33*, 157–174.
Westerhold, T., T. Bickert, and U. Röhl (2005), Middle to Late Miocene oxygen isotope stratigraphy of ODP site 1085 (SE Atlantic): New constrains on Miocene climate variability and sea-level fluctuations, *Palaeogeogr. Palaeoclimatol. Palaeoecol.*, *217*, 205–222.
Wilkens, R. H., G. R. Dickens, J. Tian, J. Backman, and the Expedition 320/321 Scientists (2013), Data report: Revised composite depth scales for Sites U1336, U1337, and U1338, in *Proc. IODP*, vol. 320/321, edited by H. Pälike et al., and the Expedition 320/321 Scientists, 158 pp., Tokyo, doi:10.2204/iodp.proc.320321.209.2013.
Winter, A., and W. G. Siesser (1994), *Coccolithophores*, 242 pp., Cambridge Univ. Press, New York.
Young, J. (1990), Size variation of Neogene *Reticulofenestra* coccoliths from Indian Ocean DSDP cores, *J. Micropalaeontol.*, *9*, 71–85.
Young, J. R., and P. Ziveri (2000), Calculation of coccolith volume and its use in calibration of carbonate flux estimates, *Deep Sea Res., Part II*, *47*(9–11), 1679–1700.
Young, J. R., J. M. Didymus, P. R. Bown, B. Prins, and S. Mann (1992), Crystal assembly and phylogenetic evolution in heterococcoliths, *Nature*, *356*, 516–518.
Ziveri, P., H. M. Stoll, I. Probert, C. Klaas, M. Geisen, J. Young, and G. Ganssen (2003), Stable isotope vital effects in coccolith calcite, *Earth Planet. Sci. Lett.*, *210*(1–2), 137–149.